Article

The control of the crossover localization in Allium

Natalia Kudryavtseva [1,2], Aleksey Ermolaev [2,3], Anton Pivovarov [1,2], Sergey Symanovskiy[4], Sergey Odintsov [1,2] and Ludmila Khrustaleva[1,2,5,*]

1 Plant Cell Engineering Laboratory, All-Russian Research Institute of Agricultural Biotechnology, Timiryazevskay 42 Str., 127550 Moscow, Russia
2 Center of Molecular Biotechnology, Russian State Agrarian University-Moscow Timiryazev Agricultural Academy (RGAU-MTAA), 49, Timiryazevskaya Str., 127550 Moscow, Russia
3 Laboratory of Applied Genomics and Crop Breeding, All-Russia Research Institute of Agricultural Biotechnology, Timiryazevskaya str. 42, Moscow 127550, Russia, All-Russia Research Institute of Agricultural Biotechnology, Moscow, Russia; ermol-2012@yandex.ru
4 Severtsov Institute of Ecology and Evolution, Russian Academy of Sciences, 33 Leninsky prosp., 119071 Moscow, Russia; sergey.a.simanovsky@gmail.com
5 Department of Botany, Breeding and Seed Production of Garden Plants, Russian State Agrarian University-Moscow Timiryazev Agricultural Academy (RGAU-MTAA), 49, Timiryazevskaya Str., 127550 Moscow, Russia
* Correspondence: ludmila.khrustaleva19@gmail.com or khrustaleva@rgau-msha.ru

Abstract: Meiotic crossovers/chiasmata are not randomly distributed and strictly controlled. The mechanisms behind COs patterning remain largely unknown. In many species COs predominantly occur in the distal 2/3 of the chromosome arm and suppression of COs is observed in the proximal regions. The exceptions are some species, among which *Allium fistulosum* has strictly localized COs in the proximal region. The ability to manipulate the COs localization can be useful for onion breeding. We investigated the factors that may contribute to the pattern of COs in two closely related onion species *A. cepa* and *A. fistulosum*, which differ significantly in the localization of chiasmata, and their F_1 diploid and triploid hybrids in pollen mother cells. We demonstrate a significant shift in the COs localization to the distal and interstitial region in F_1 triploid hybrid, which has a complete diploid set of *A. fistulosum* chromosomes and haploid set of *A. cepa* chromosomes. This observation points to a possible genetic control of COs distribution. We did not find the differences in the assembly and disassembly of ASY1 and ZYP1 between *A. cepa* and *A. fistulosum* while the difference between parental species and their hybrids was observed. In diploid F_1 hybrids at pachytene the chromosome pairing delay marked by ASY1 was revealed. Immunolocalization of MLH1, a marker for class I of the interference-dependent COs, and MUS81, a marker for class II of the interference-free COs, and *mlh1/mus81* gene expression profiling in different stages of meiosis showed a spatiotemporal asymmetry among *A. cepa*, *A. fistulosum* and their diploid and triploid F_1 hybrids. Our results support the hypothesis of genetic control of CO distribution as one of the players that affect meiotic recombination and exchange of genomic material.

Keywords: chiasama distibution; *mus81*; *mlh1*; ASY1; ZYP1; synaptonemal complex; Allium; GISH; expression profiling

1. Introduction

Meiotic crossovers (recombination) in plants are not distributed randomly along the length of individual chromosomes and are tightly regulated [1–5]. Crossovers (COs) most often occur in the distal 2/3 of the chromosome arm, while suppression of recombination is observed in the proximal centromere regions in most eukaryotes. The exceptions are some species, among which *Allium fistulosum* has strictly localized COs in the proximal region adjacent to the centromere [6]. COs can be visualized cytologically as chiasmata that promote accurate segregation of homologous chromosomes, which is a key moment in the formation of the chromosome set of gametes. It is obvious that the formation of

 doi:10.20944/preprints202212.0307.v1

COs is strictly controlled to prevent the appearance of non-exchange chromosomes [7–9]. At the same time with obligate recombination (1-2 per bivalent), COs are not randomly distributed along the chromosome. The phenomenon of interference discovered at the beginning of the last century [10,11] is one of the evidence indicating the existence of control over the formation of COs. Interference refers to the observation that a CO in one region of chromosome interferes another CO to be formed nearby. COs are generated by homologous recombination initiated by DNA double-strand breaks (DSBs) formed by the topoisomerase-like SPO11 protein [12]. There are DSBs substantially more that crossovers [13]. DSBs that do not become crossovers are repaired to give non-crossovers. According to yeast study, COs tend to form with an excess of non-crossovers [14]. The authors suggested that obligate crossing over is a genetically programmed event associated with crossing over interference. Earlier in the era of classical genetics, the hypothesis of a possible genetic control of the distribution of chiasmata was advanced by Emsweller and Jones [15]. The authors were intrigued by the different localization of chiasmata in two closely related Allium species. In *A. cepa*, the chiasmata are localized in the distal and interstitial regions and appear as ring bivalents, while in *A. fistulosum*, on the contrary, the chiasmata are strictly located in the proximal region and appear as cross bivalents. Analyzing the meiosis of an F_1 hybrid between *A. cepa* and *A. fistulosum*, Emsweller and Jones found that all the bivalents were ring as in *A. cepa*. When F_1 hybrid was backcrossed with *A. fistulosum*, the ring and cross bivalents at metaphase I stage were close to the 1:1 ratio [16]. The authors suggested that the localization of chiasmata is apparently determined by a single gene: in *A. fistulosum* it is a recessive gene, while in *A. cepa*, it is a dominant gene. Today, in the post-genomic era, many factors are being considered to explain the phenomenon of non-random localization of COs. The meiotic recombination pathway begins with each chromosome binding to a protein axis that includes ASY1, the lateral element of the synaptonemal complex (SC) at leptotene [17], and then programmed induction of DNA double-strand breaks (DSBs) occurs. By mapping ASY1 enrichment using chromatin immunoprecipitation sequencing (ChIP-seq) in wild type and asy mutants in *Arabidopsis thaliana* was shown that in the absence of ASY1 telomere-led recombination becomes dominant [18]. ZIP1 protein, the component of central element of SC a play role of a molecular zipper to bring homologous chromosomes in close apposition and synapsis formation [19–21]. Recent studies in plants showed, that ZYP1 may be key players to control the number and location of meiotic crossovers [22]. ZIP1 is absolutely required for Class I crossover formation in yeast [23] while in Arabidopsis and rice, ZYP1 are dispensable Class I crossover formation [20,21,24]. There are two classes of crossovers: class I crossovers that are subject to interference and class II that are indifferent to interference [25–27]. Class I COs (interference depended) require many proteins including the ZMM group (ZIP1-4, MSH4-5, MER3) and the MutL homolog 1 (MLH1)/MLH3 complex [25,28]. class II depends primarily on the Mus81/Mms4 endonuclease complex in budding yeast [26,29]. Analysis of *Atmsh4/Atmus81* double mutant revealed a significantly reduced mean chiasma frequency (0.85 per cell), compared with an Atmsh4 single mutant (1.25 per cell) [30]. The authors suggested that AtMUS81 accounts for some, but not all, of the 15% AtMSH4-independent residual crossovers. It has recently been found that Class II COs can be generated by at least two parallel pathways in Arabidopsis which depend on either the structure-specific endonuclease AtMUS81 or a homolog of Fanconi Anemia Complementation Group D2 (*AtFANCD2*) that promotes noninterfering COs [31].

Mapping the physical distribution of COs along pachytene chromosomes is an important step toward understanding the regulation of crossing over. Using combination of immunefluorescent localization of meiotic proteins and SC spreads Anderson and coauthors [32] showed that class I and class II COs have different recombination profiles along chromosome. Notably, class II COs was mostly located in pericentric heterochromatin. MLH1 is endonuclease that actives in resolving recombination intermediates and in DNA mismatch repair. Antibody to MLH1 is often used for localization of class I COs in plants (Arabidopsis, wheat, tomatoes) [33–36] as well as in mammals [37–39] MUS81 indicates

 doi:10.20944/preprints202212.0307.v1

COs that may be formed by the processing of non-Holliday junction (HJ) intermediates and involved in a secondary subset of meiotic crossovers that are interference insensitive [40–42]. The MUS81 were used for immunolocalization of interference-insensitive COs (class II) in wheat [43] and mammals [39].

In this study, we investigated the factors that may contribute to the pattern of recombination in two closely related onion species that differ significantly in the localization of chiasmata in Pollen Mother Cells (PMCs). *A. fistulosum* is a rich reservoir of desirable traits for improving the bulb onion (*Allium cepa*) gene pool [16,44,45]. Knowing the CO distribution may assist when attempting the introgression new genetic traits. The ability to manipulate the distribution of chiasmata could be valuable for onion breeding. Our study is based on an advanced approach that uses a comparative analysis of chiasma distribution in PMCs, immunolocalization of MLH1, MUS81, ASY1 and ZYP1 on meiotic chromosomes, and *mlh1/mus81* gene expression profiling in different stages of meiosis in *A. fistulosum*, *A. cepa* and diploid (2n = *2x* = 8C+8F) and triploid (2n = *3x* = 16F+8C) F_1 hybrids *A. cepa* × *A. fistulosum*. We demonstrate a significant shift in the localization of chiasmata to the distal and interstitial region in F_1 triploid hybrid, which have a complete diploid set of *A. fistulosum* chromosomes and haploid set of *A. cepa* chromosomes. This observation points to a possible genetic control of chiasma distribution. Immunocytochemistry using a panel of antibodies against meiotic proteins and *mlh1* and *mus81* genes expression profiling in different stages of prophase I revealed a spatiotemporal asymmetry among *A. cepa*, *A. fistulosum* and their diploid and triploid F_1 hybrids.

2. Results

2.1. GISH analysis of genomic structure of F_1 hybrids A. cepa × A. fistulosum

Scoring of chromosome number in F_1 hybrids on mitotic metaphase spreads revealed the presence of individual plants with 16 and 24 chromosomes. GISH analysis showed that the F_1 hybrid acc. 1-20 with 16 chromosomes displayed 8 chromosomes of *A. cepa* (8C) and 8 chromosomes of *A. fistulosum* (8F) (Figure 1a). Karyotype analysis showed the presence of complete haploid sets of both parental species: 2n = *2x* = 8F + 8C (Figure 1a'). GISH analysis of F_1 hybrid acc. 7-20 with 24 chromosomes displayed 8 chromosomes of *A. cepa* (8C) and 16 chromosomes of *A. fistulosum* (16F) (Figure 1b). Karyotype analysis showed the presence of complete haploid set of *A. cepa* and complete diploid sets of *A. fistulosum* chromosomes: 2n = *3x* = 16F+8C (Figure 1b'). The GISH result indicates the formation of unreduced 2n-gametes during microspogenesis in *A. fistulosum*. The triploid hybrid is a unique plant material for studying the effect of the *A. cepa* haploid genome on the configuration of the *A. fistulosum* homologous bivalents, assembly and disassembly of synaptonemal complex, MLH1 and MUS81 protein localization, and *mlh1* and *mus81* gene expression during prophase I of meiosis.

2.2. The chiasma distribution in PMCs at metaphase I

Previously, it was thought that distal chiasmata may have originated in more central regions of chromosomes and migrated by a process called terminalization to distal regions but now it is known that chiasmata do not terminate and therefore their location reflects their real place of origin [46–48].

The acetocarmine stained squash preparations of pollen mother cells (PMCs) at metaphase I of *A. cepa*, *A. fistulosum* and their F_1 diploid and triploid hybrids were analyzed. In *A. cepa* chiasmata occurred mainly in distal and interstitial bivalent regions and very rare in proximal regions. The vast majority of metaphases contained eight bivalents with two distal chiasmata, and bivalents with three chiasmata were also often encountered, especially in long chromosomes, in which two distal and one interstitial chiasmata occurred (Figure 2a). The extreme localization of chiasmata to the proximal regions adjacently to centromere of the *A. fistulosum* bivalents was evident, although occasionally distal and interstitial chiasmata and univalents were found (Figure 2b).

Preprints (www.preprints.org) | NOT PEER-REVIEWED | Posted: 16 December 2022 doi:10.20944/preprints202212.0307.v1

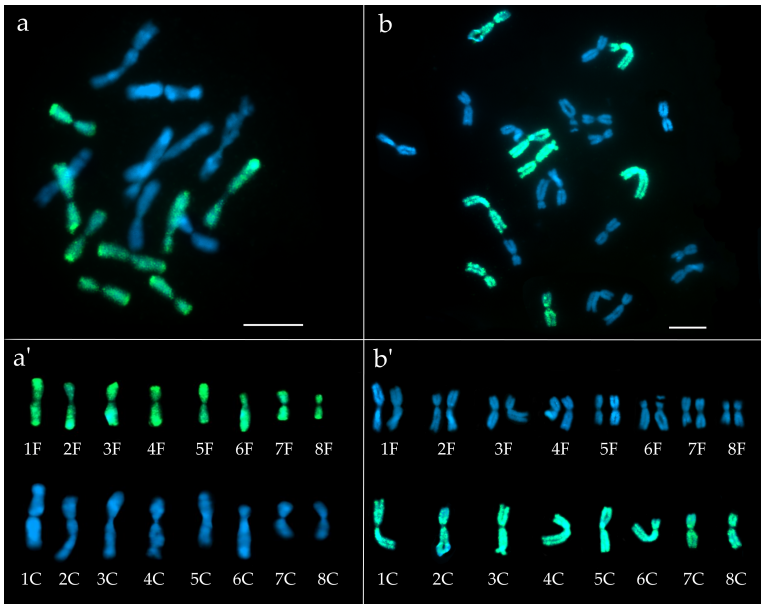

Figure 1. GISH on mitotic metaphase chromosomes of interspecific hybrids between *A. cepa* and *A. fistulosum*: (a) diploid hybrid contains 8 chromosomes of *A. cepa* and 8 chromosomes of *A. fistulosum*; (b) triploid hybrid contains 8 chromosomes of *A. cepa* and 16 chromosomes of *A. fistulosum*; (a',b') karyotypes of the diploid and triploid hybrids respectively.

In diploid F_1 hybrids *A. cepa* × *A. fistulosum*, carrying eight chromosomes of the *A. cepa* female parental species and eight chromosomes of the *A. fistulosum* male parental species, the chiasma distribution was most similar to that of the *A. cepa* parent. No bivalents were observed with only proximally localized chiasmata as in *A. fistulosum*. The bivalents formed by this hybrid possessed chiasmata mostly in distal and interstitial regions. This shows that homoeologues paired during prophase I of meiosis and that there was sufficient homology to allow chiasma formation. *A. fistulosum* and *A. cepa* differ in genome size, *A. cepa* (1C = 16.4 Gb, [49]) having 4.8 Gb more DNA and correspondingly larger chromosomes than *A. fistulosum* (1C = 11.6 Gb, [50]). We have observed heteromorphic bivalents, open bivalents with one chiasma and univalent pair of unequal size (Figure 2c). The chiasmata frequencies and distributions in *A. cepa*, *A. fistulosum* and their F_1 hybrids are presented in Tables 1. In F_1 hybrid 47.7% chiasmata were located in distal bivalent regions and 41.3 in interstitial one, which is considerably higher than that of *A. fistulosum* (1.7% and 1.2%, correspondingly).

In F_1 triploid hybrids, which have a complete diploid set of *A. fistulosum* chromosomes and eight chromosomes of the female parental species *A. cepa*, we were able to analyze the morphology of bivalents formed by homologous chromosomes of *A. fistulosum* in the presence of a complete haploid set of the *A. cepa* chromosomes. Pairs of the *A. fistulosum* homologous chromosomes formed bivalents with distal and interstitial localization of chiasmata: 34.5% chiasmata were located in distal bivalent regions and 26.0% in interstitial one (Table 1). This might indicate the presence of a dominant gene in A cepa, which determines the position of the chiasmata. Although bivalents with two proximal chiasmata were observed, which is typical for *A. fistulosum* (Figure 2d).

Chiasmata of both parental onion spices tend to arise in favored chromosomal regions, namely, in proximal region of *A. fistulosum* and distal region of *A. cepa*, However, such a pronounced local distribution of chiasmata was not observed in hybrids between *A. fistulosum* and *A. cepa*, where the position of chiasmata along the chromosomes was quite variable from cell to cell. In F_1 diploid hybrid, an individual cell with 6 chiasmata in the interstitial region, 9 — distal and none chiasmata in the proximal region along with, a cell with 2 chiasmata proximal, 6 - interstitial and 9 — distal was found. In F_1 triploid hybrid, an individual cell with 10 chiasmata in the proximal region, 1 — interstitial and 6 — distal along with, a cell with 2 chiasmata proximal, 11 — interstitial and 3 — distal was revealed.

Preprints (www.preprints.org) | NOT PEER-REVIEWED | Posted: 16 December 2022 doi:10.20944/preprints202212.0307.v1

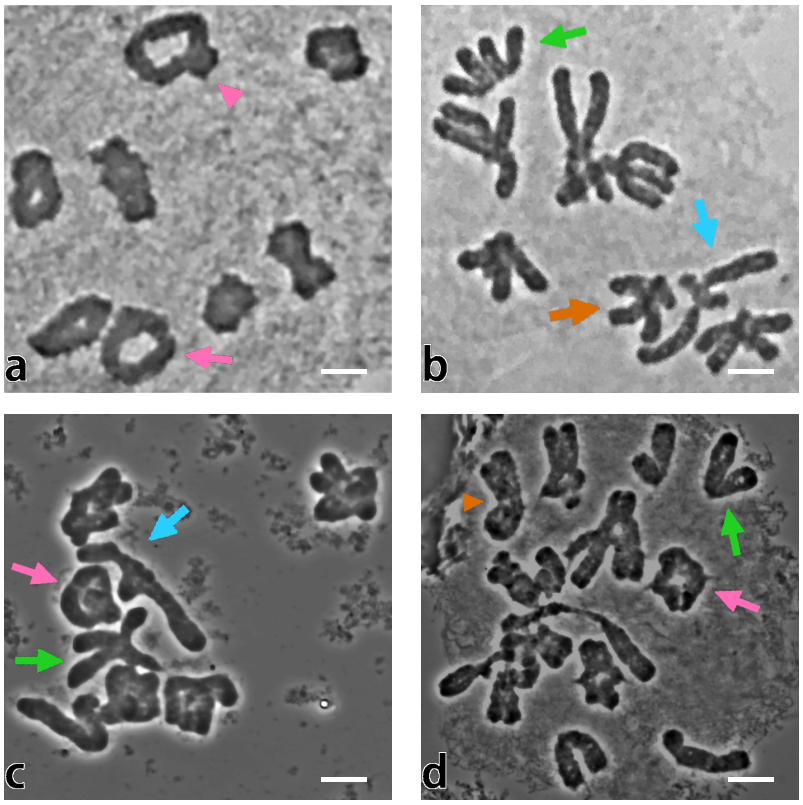

Figure 2. Acetocarmine-stained squash preparations of PMCs at metaphase I: a — *A. cepa*, b — *A. fistulosum*, c — F_1 *A. cepa* × *A. fistulosum* (2n = 2*x* = 8F+8C) and d — triploid *A. cepa* × *A. fistulosum* (2n = 3*x* = 16F+8C). Pink arrow indicates bivalent with two distal chiasmata (arrow head – bivalent with two distal and interstitial chiasmata); blue arrow indicates open bivalent with one interstitial chiasma; orange arrow indicates univalent. Note the heteromorphic bivalents and univalent pair of unequal size (c), and eight univalent belonged to *A. cepa* (d). Bars represent 10 μm.

The data of chiasma distribution in *A. cepa*, *A. fistulosum* and their F_1 diploid and triploid hybrids presented in Table 1 we analyzed using a multivariate statistical method (correspondence analysis) that provides a means of displaying a set of data in two-dimensional graphical form — biplot (Figure 3). According to the correspondence analysis there is a three groups into which analyzed samples can be assigned. *A. cepa* and *A. fistulosum* can be considered as a two different groups whereas both hybrid F_1 *A. cepa* × *A. fistulosum* (8C+8F) and triploid *A. cepa* × *A. fistulosum* (8C+16F) are separated and forms another group. Distance between points on a biplot is a measure of similarity of observations. Based on distance between points we can conclude that diploid F_1 hybrid *A. cepa* × *A. fistulosum* (8C+8F) and triploid F_1 hybrid *A. cepa* × *A. fistulosum* (8C+16F) are more similar to *A. cepa*.

2.3. Behavior of ASY1 and ZYP1 during SC assembly and disassembly in A. cepa, A. fistulosum and their diploid and triploid F_1 hybrids

The dynamics of the synaptonemal complex (SC) during prophase I was monitored by immunolocalization of ASY1 (lateral elements of SC) and ZYP1 (transverse filaments of SC). At leptotene of *A. cepa*, ASY1 loaded on the meiotic chromosome axes, while ZYP1 began to be loaded along the synapse sites. At zygotene, ASY1 was detected as single thin tracks that corresponded to unpaired chromosome axes, while ZYP1 tracks became more longer along synapsed chromosome axes. At pachytene, ZYP1 tracks have fully formed along the synapsed homologous chromosomes, while only a few unpaired regions can be identified by some weak ASY1 signals or as a remaining diffuse signal. During diplotene, ZYP1 undergoes degradation indicating the beginning of disassembly of synaptonemal complexes. At diakinesis, ZYP1 signals are appear as ball-like structures (Figure 4).

Preprints (www.preprints.org) | NOT PEER-REVIEWED | Posted: 16 December 2022 doi:10.20944/preprints202212.0307.v1

Table 1. Chiasma frequency and distribution in *A. cepa*, *A. fistulosum*, and the F_1 hybrid *A. cepa* × *A. fistulosum*.

	Number of cells scored	Mean PMC chiasma frequency	Number of bivalents analyzed	Chiasma location					
				Proximal		Interstitial		Distal	
				%	(total)	%	(total)	%	(total)
A. cepa	54	19.1	435	1.8	(18)	20.0	(207)	78.2	(808)
A. fistulosum	43	15.4	340	97.1	(643)	1.2	(8)	1.7	(11)
F_1 *A. cepa* × *A. fistulosum* (2n = 2*x* = 8F+8C)	35	12.0	248	11.4	(48)	43.0	(180)	45.6	(191)
F_1 *A. cepa* × *A. fistulosum* (2n = 3*x* = 16F+8C)	29	14.6	231	39.5	(167)	26.0	(110)	34.5	(146)

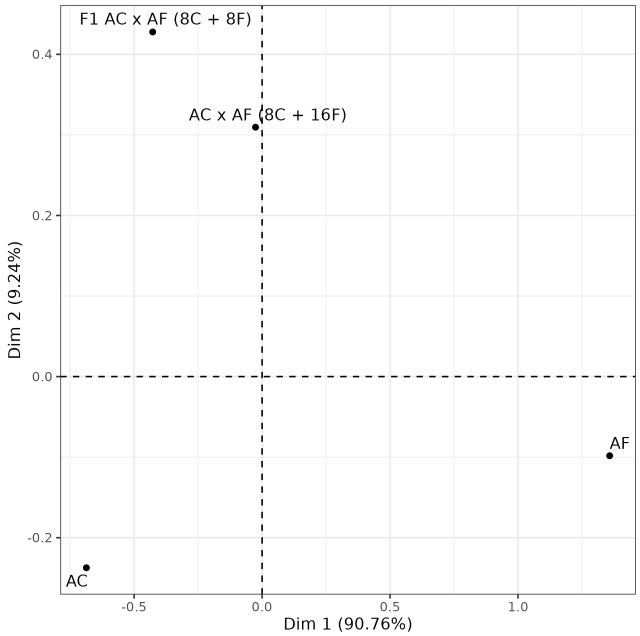

Figure 3. A biplot of the correspondence analysis of the distribution of chiasmata by chromosomal regions (proximal, interstitial, distal) in *A. cepa*, *A. fistulosum*, F_1 *A. cepa* × *A. fistulosum* (2n = 2*x* = 8F+8C) and F_1 *A. cepa* × *A. fistulosum* (2n = 3*x* = 16F+8C).

In PMCs of *A. fistulosum*, behavior of ASY1 and ZYP1 was similar to the *A. cepa*. We did not find any differences in the assembly and disassembly processes of these proteins between *A. cepa* and *A. fistulosum* (Figure 5).

In F_1 diploid hybrids, behavior of ASY1 and ZYP1 was similar to *A. cepa* and *A. fistulosum*, except for a longer pairing process. At pachytene, a large number of unpaired regions with ASY1 tracks between homeologous chromosomes were observed (Figure 6).

In F_1 triploid hybrid, the unpaired ASY1 tracks were present at pachytene, which can be explained more by the presence of an unpaired set of *A. cepa* chromosomes (8C) than by the remaining unpaired homologous chromosomes of *A. fistulosum* (16F) (Figure 7).

2.4. Immunocytological detection of MLH1, MUS81 and CENH3 on the pachytene chromosomes of A. cepa and A. fistulosum, and their hybrids

To analysis the localization MLH1 and MUS81 in onions, the protocol of simultaneous immunostaining with both antibodies to MLH1 and MUS81 was developed. To determine relative position of MLH1 and MUS81 foci to centromere we used sequential immunostaining with antibodies to CENH3 on the same pachytene chromosome (see Materials and Methods). The numbers of MLH1 foci per cell in *A. cepa* was higher (mean = 6.0, n = 9) compared to *A. fistulosum* (mean = 2.2, n = 9) that showed a significant difference ($t_{(16)}$ =

Preprints (www.preprints.org) | NOT PEER-REVIEWED | Posted: 16 December 2022 doi:10.20944/preprints202212.0307.v1

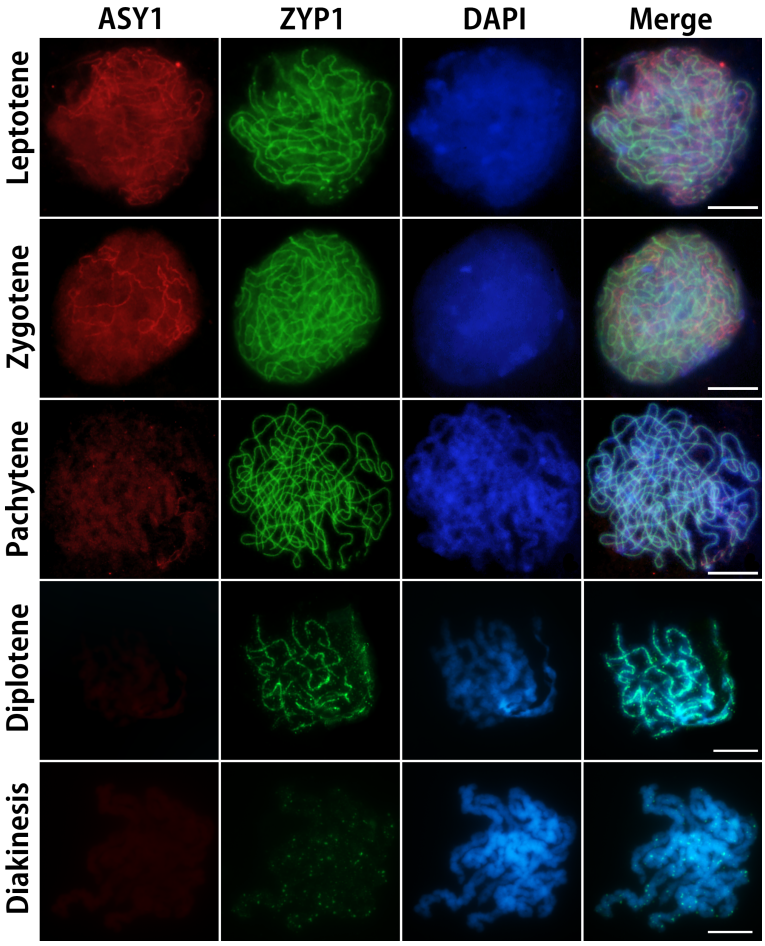

Figure 4. The behavior of ASY1 (red) and ZYP1 (green) during prophase I in *A. cepa*. Chromatin was stained with DAPI. Bar = 10 μm.

3.48, P = 0.006). The numbers of MUS81 foci per cell in *A. cepa* was lower (mean = 2.3, n = 9) compared to *A. fistulosum* (mean = 5.6, n = 9) that showed a significant difference ($t_{(16)}$ = -5.04, P = 0.001). In *A. cepa* the ratio of mean number of MLH1:MUS81 foci per cell was about 3:1 while the MLH1:MUS81 ratio in *A. fistulosum* was vise verse about 3:1.

In *A. cepa* and *A. fistulosum* were difficult to analyze of individual chromosomes at pachytene. We were able to determine the chromosomal localization of MLH1 and MUS81 and measure a relative distance to the centromere on a limited number of chromosomes. In *A. cepa*, the MLH1 foci were located in interstitial and distal regions of chromosomes and MUS81 foci were observed in interstitial region. In *A. fistulosum*, MLH1 foci was located mainly in interstitial and distal regions and very rare in proximal region, while MUS81 foci were observed in proximal regions of chromosomes (Figure 8). In some chromosomes the centromere was flanked by two MUS81 fluorescent signals, while in the other chromosomes the centromere had a MUS81 foci on one side.

In *A. cepa*, two chromosomes in one pachytene cell with clear MLH1 and CENH3 signals were used for measuring distance between them. The distance between MLH1 and centromere on the first chromosome ~12.7 nm. The distance between MLH1 and CENH3 of the other chromosome ~12.8 nm. In one pachytene of *A. fistulosum*, the chromosome with MUS81 foci very close to the centromere (~1 nm) was found. The distance between MUS81 and CENH3 on the other chromosome was ~3 nm.

In diploid F_1 hybrids, the mean number of MLH1 foci per cell was 4.5 (n = 8), while the mean number of MUS81 foci was 5.8 (n = 8). The mean number of MLH1 foci per cell in diploid F_1 hybrids was lower than in the *A. cepa*, but this difference was not statistically significant (4.5 versus 6.0 MLH1 foci per cell, $t_{(15)}$ = 1.23, P = 0.242). The mean number

Preprints (www.preprints.org) | NOT PEER-REVIEWED | Posted: 16 December 2022 doi:10.20944/preprints202212.0307.v1

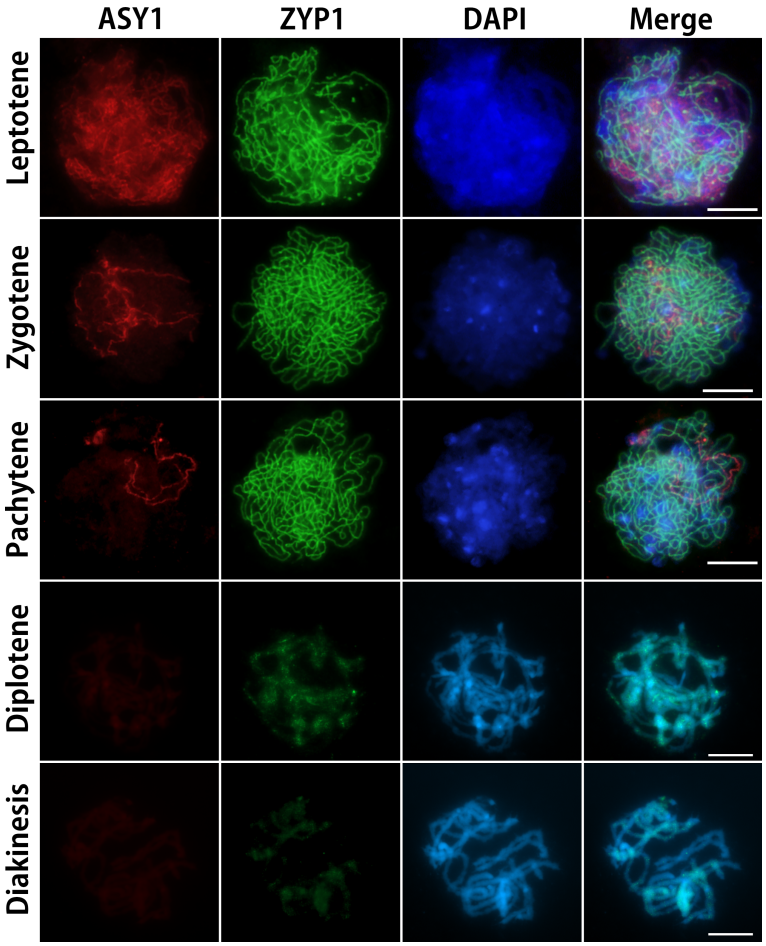

Figure 5. The behavior of ASY1 (red) and ZYP1 (green) during prophase I in *A. fistulosum*. Chromatin was stained with DAPI. Bar = 10 μm.

of MLH1 foci per cell in F_1 diploids was higher than in *A. fistulosum*, and this difference was statistically significant (4.5 versus 2.2 MLH1 foci per cell, $t_{(15)}$ = -4.55, P = 0.001). The mean number of MUS81 foci per cell in the F_1 diploids was higher than in *A. cepa*, and this difference was statistically significant (5.8 versus 2.3 MUS81 foci per cell, $t_{(15)}$ = -3.68, P = 0.003), while the mean number of MUS81 foci per cell in the F_1 diploids did not vary significantly compared to *A. fistulosum* (5.8 versus 5.6 MUS81 foci per cell, $t_{(15)}$ = -0.13, P = 0.902). MLH1 foci were located in interstitial and distal regions, while MUS81 were located in proximal and interstitial and very rare in distal regions. Two signals from MLH1 and MUS81 on the same chromosome in pachytene was observed (Figure 8). The distance between MLH1 and MUS81 foci was ~1.8 nm.

In triploid F_1 hybrids *A. cepa* × *A. fistulosum* the mean number of MLH1 foci per cell was 4.3 (n = 8), while the mean number of MUS81 foci was 3.1 (n = 8). The mean number of MLH1 foci per cell in F_1 triploids did not vary significantly compared to *A. cepa* (4.3 versus 6.0 MLH1 foci per cell, $t_{(15)}$ = 1.67, P = 0.119), while the mean number of MLH1 foci per cell in F_1 triploids was higher than *A. fistulosum* (4.3 versus 2.2 MLH1 foci per cell), and this difference was statistically significant ($t_{(15)}$ = -2.42, P = 0.034). The mean number of MUS81 foci per cell in F_1 triploids did not vary significantly compared to *A. cepa* (3.1 versus 2.3 MUS81 foci per cell, $t_{(15)}$ = -1.30, P = 0.217), while the mean number of MUS81 foci per cell in F_1 triploids was lower than in *A. fistulosum* (3.1 versus 5.6 MUS81 foci per cell), and this difference was statistically significant ($t_{(15)}$ = 2.82, P = 0.017). The mean number of MLH1 foci per cell in F_1 triploids did not vary significantly compared to F_1 diploids (4.3 versus 4.5 MLH1 foci per cell, $t_{(15)}$ = 0.85, P = 0.410), while the mean number of MUS81 foci per cell in F_1 triploids was lower than in F_1 diploids (3.1 versus 5.8 MUS81 foci per

Preprints (www.preprints.org) | NOT PEER-REVIEWED | Posted: 16 December 2022 doi:10.20944/preprints202212.0307.v1

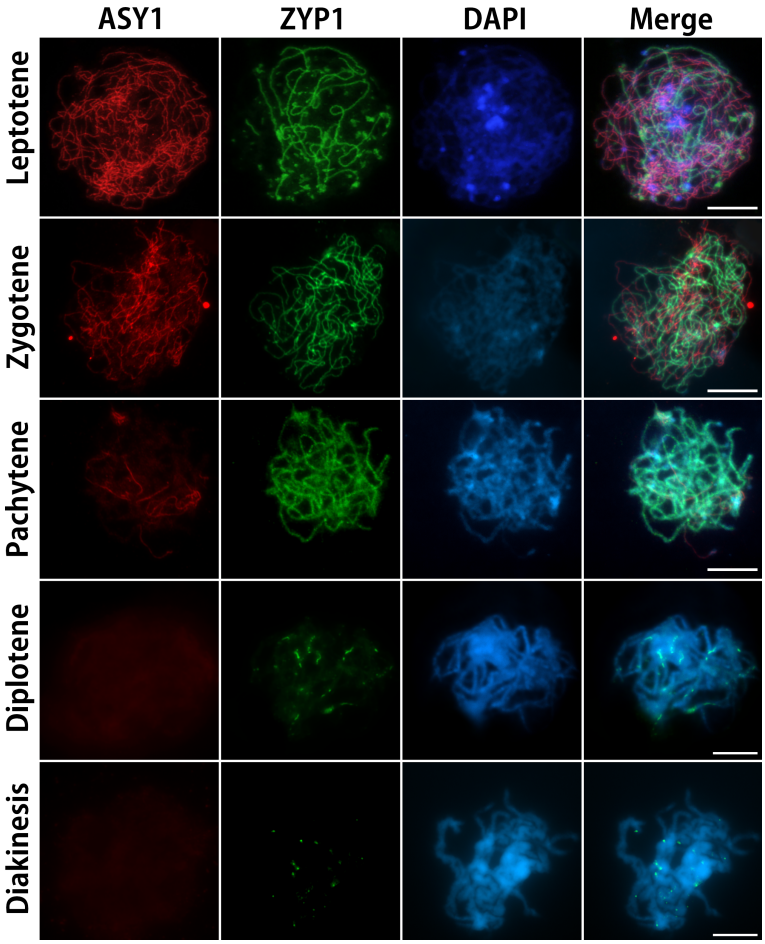

Figure 6. The behavior of ASY1 (red) and ZYP1 (green) during prophase I in F_1 diploid hybrid *A. cepa* × *A. fistulosum* (2n = 2*x* = 8F+8C). Chromatin was stained with DAPI. Bar = 10 μm.

cell) and this difference was statistically significant ($t_{(15)}$ = 2.62, P = 0.020). The MLH1 were located mainly in interstitial and distal regions and very rare in proximal regions, while MUS81 were located in proximal and interstitial and very rare in distal regions. The cromosomes carring the MUS81 foci to the centromere were found in F_1 triploid as well as in *A. fistulosum*.

2.5. Gene expression profiling with a droplet digital PCR assay

We measured the absolute copy number (CN) of *mus81* and *mlh1* in different stages of prophase I of meiosis (leptotene, zygotene and pachytene) in *A. cepa* (16C), *A. fistulosum* (16F), F_1 hybrid *A. cepa* × *A. fistulosum* (8F+8C) and triploid *A. cepa* × *A. fistulosum* (16F+8C) using highly sensitive method for absolute quantification of DNA molecules in sample — digital PCR. Data about measurments of the CN of *mus81* and *mlh1* in different samples (species, meiosis stage) as well as meiosis by-stage profiling are represented in Table 2 and Figure 9, respectively.

Copy number of *mus81* is 1.6-fold more than *mlh1* in leptotene of *A. cepa* whereas in leptotene of *A. fistulosum* the CN of these transcripts are almost equal. *mus81* in leptotene of *A. cepa* shows 2.9-fold higher CN than in leptotene of *A. fistulosum* whereas fold change of CN of *mlh1* between species is 1.8. In comparison with leptotene, in the zygotene the CN of *mlh1* of *A. cepa* increasing in 2.3-fold while CN of *mus81* remains almost the same (1.2-fold change). In *A. fistulosum* both transcripts showed the same fold change in the zygotene in comparison with the leptotene (2.4-fold). The CN of *mus81* in zygotene of *A. cepa* is 1.4-fold higher than in zygotene of *A. fistulosum* whereas fold change of *mlh1* is 1.8. In the pachytene of *A. cepa* and *A. fistulosum* in comparison with the zygotene observed dramatic

 doi:10.20944/preprints202212.0307.v1

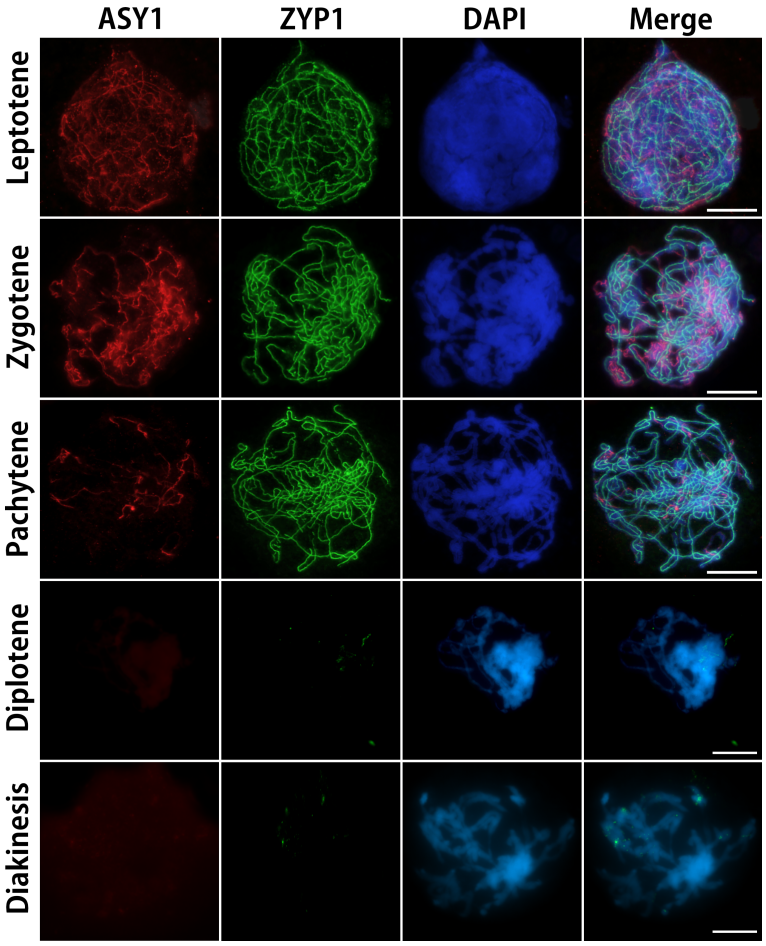

Figure 7. The behavior of ASY1 (red) and ZYP1 (green) during prophase I in F_1 triploid hybrid *A. cepa* × *A. fistulosum* (2n = 2*x* = 16F+8C). Chromatin was stained with DAPI. Bar = 10 μm.

decreasing of CN both *mlh1* and *mus81* — 2.3-fold change of *mus81* and 3.8-fold change of *mlh1* in *A. cepa*, and 3.1-fold change of both *mlh1* and *mus81* in *A. fistulosum*. Both *A. cepa* and *A. fistulosum* showed similar patterns of CN changing in the course of prophase I of meiosis (Figure 9): the maximum CN is observed in zygotene while both in leptotene and pachytene the CN is decreasing.

In the leptotene of the F_1 diploid hybrid the values of CN of *mlh1* and *mus81* as well as ratio of CNs of *mus81* to *mlh1* (0.8) is closer to *A. fistulosum* values (1.0) rather than *A. cepa* (1.6). In the zygotene of the F_1 diploid hybrid both transcripts has higher values of the CN (1.6-fold change for *mus81* and 1.8-fold change for *mlh1*) in comparison with leptotene. The ratio of the CN of *mus81* to *mlh1* in zygotene of hybrid is 0.7 which is closer to *A. cepa* ratio (0.8) rather than *A. fistulosum* (1.1). The absolute CN values of *mus81* and *mlh1* in zygotene of the F_1 diploid hybrid are smaller than both in *A. cepa* (2.3-fold change both for *mus81* and *mlh1*) and *A. fistulosum* (2.0-fold change for *mus81* and 1.3-fold change for *mlh1*). Both *mus81* and *mlh1* CNs continues to increase in pachytene of the F_1 diploid hybrid in comparison to zygotene (2.4-fold change for *mus81* and 1.9-fold change for *mlh1*). By-stage pattern of both *mlh1* and *mus81* in the F_1 diploid hybrid differ both from *A. cepa* and *A. fistulosum*: the CN values of both *mlh1* and *mus81* shows constant increasing in the course of prophase I of meiosis and reached the maximum in pachytene rather than in zygotene (Figure 9).

In the leptotene of the triploid the ratio CNs of *mus81* to *mlh1* significantly lower *A. cepa*, *A. fistulosum* and the F_1 diploid hybrid: triploid showed 0.3 CN ratio while the ratio in *A. cepa* and *A. fistulosum* is almost equal or higher than 1 (1.6 for *A. cepa* and 1.0 for *A. fistulosum*) whereas in the F_1 diploid hybrid the decreasing of the CN ratio is observed (0.8). *mus81* CN of the triploid is closer to *A. fistulosum* CN (0.8-fold change) rather than

Preprints (www.preprints.org) | NOT PEER-REVIEWED | Posted: 16 December 2022 doi:10.20944/preprints202212.0307.v1

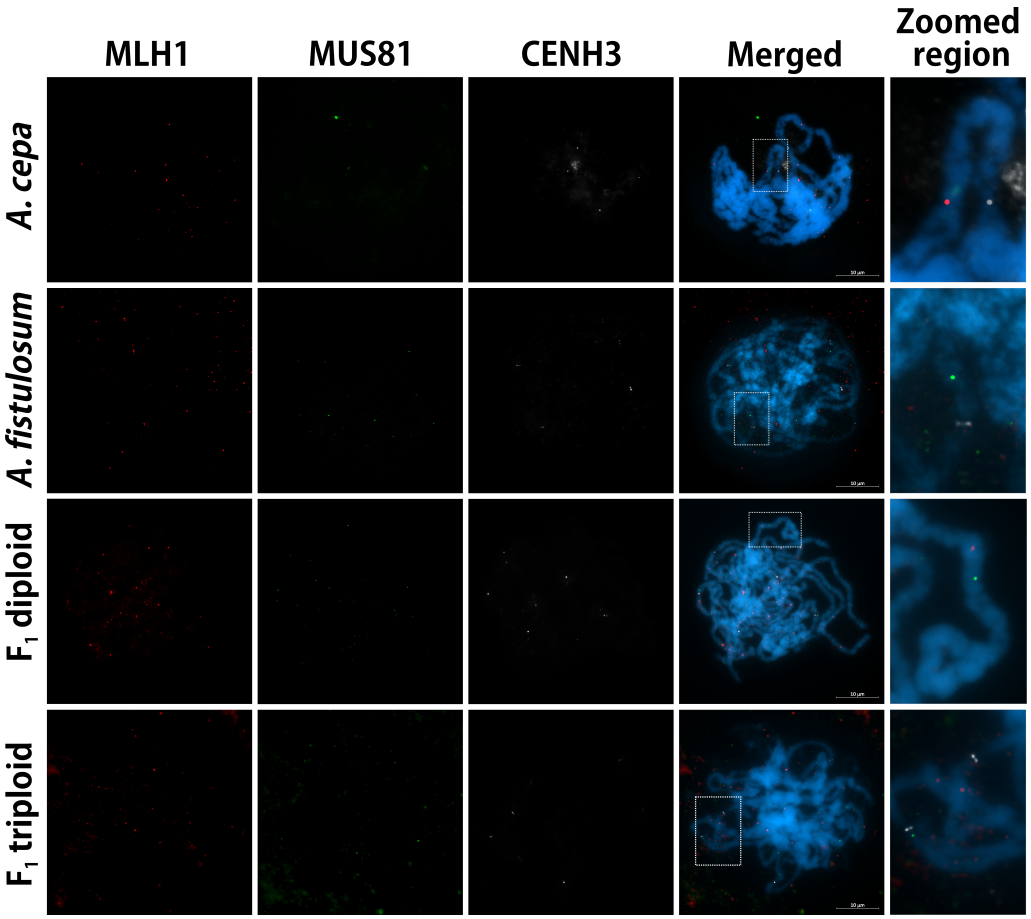

Figure 8. Immunolocalization of the MLH1, MUS81 and CENH3 on the same pachytenes of *A. cepa*, *A. fistulosum* and their hybrids. MLH1 marks class I COs (red) and MUS81 marks class II COs (green), CENH3 marks centromere (white). Chromatin was stained with DAPI. The region delimited by dashed boxes represented in zoomed region. Bar = 10 μm.

A. cepa (0.3-fold change) and almost identical to the F_1 diploid hybrid (1.1-fold change) while the CN of *mlh1* in triploid is closer to *A. cepa* CN (1.3-fold change) rather than both *A. fistulosum* and the F_1 diploid hybrid (2.4-fold change). In zygotene observed contrast behavior of CN for both *mus81* and *mlh1*: *mus81* CN is increased (1.3-fold change) while *mlh1* CN is decreased (0.7-fold change). The CN ratio of *mus81* to *mlh1* (0.7) in zygotene is closer to *A. cepa* (0.8) rather than to *A. fistulosum* (1.1) and equal to the F_1 diploid hybrid. In pachytene the CN of *mus81* almost did not change (1.1-fold change) while the CN of *mlh1* is keeping to decrease (0.8-fold change) and the CN ratio of *mus81* to *mlh1* become almost equal (0.9) which is closer to *A. fistulosum* (1.1) rather than to *A. cepa* (1.4). By-stage expression pattern of *mlh1* in triploid is differ from both *A. cepa* and *A. fistulosum* and contrast to the F_1 diploid hybrid: maximum CN is observed in leptotene and keep decreasing in the course of prophase I of meiosis. On the other hand, by-stage expression pattern of *mus81* in triploid shows the slowest but steady increasing from leptotene to pachitene stage (Figure 9).

3. Discussion

In this paper, for the first time, the analysis of the frequency and localization of chiasmata in the *A. fistulosum* homologous bivalents in the presence of a complete haploid set of the *A. cepa* chromosomes were performed. A comprehensive study of homeologous bivalents in prophase I on the spreads of synaptonemal complex (SC) and the squashed chromosome slides at metaphase I of the *A. cepa* × *A. fistulosum* F_1 diploid hybrid and its parental species has previously been reported by Albini and Jones [6,51,52]. Comparing the

Preprints (www.preprints.org) | NOT PEER-REVIEWED | Posted: 16 December 2022 doi:10.20944/preprints202212.0307.v1

Table 2. Abundance of *mus81* and *mlh1* transcripts on a different stages of meiosis based on results of ddPCR.

Meiosis stage	*Allium cepa*		*Allium fistulosum*		*Hybrid (8C+8F)*		*Triploid (8C+16F)*	
	***mus81*, copies/μL**	***mlh1*, copies/μL**	***mus81*, copies/μL**	***mlh1*, copies/μL**	***mus81*, copies/μL**	***mlh1*, copies/μL**	***mus81*, copies/μL**	***mlh1*, copies/μL**
Leptotene	138	86	48	47	36	47	38	111
Zygotene	166	199	117	111	58	86	48	72
Pachytene	72	52	38	36	138	166	52	59

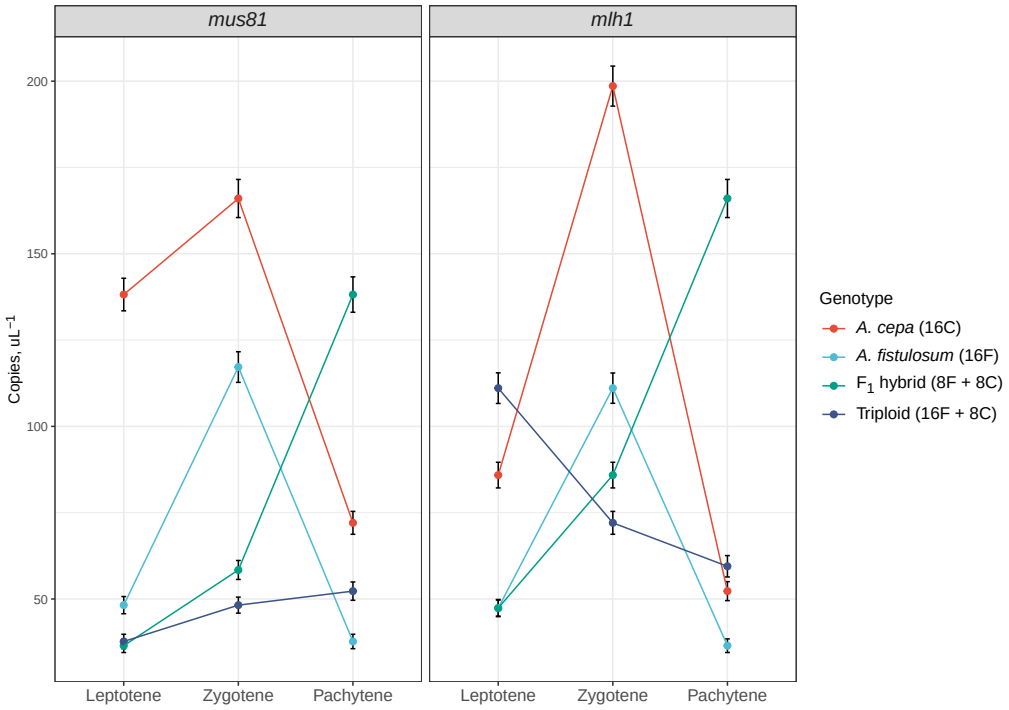

Figure 9. Temporal expression profile of *mus81* and *mlh1* genes in leptotene, zygotene and pachytene of *A. cepa*, *A. fistulosum*, F_1 hybrid *A. cepa* × *A. fistulosum* and triploid *A. cepa* × *A. fistulosum*. Copy number represented on the Y-axis. Error bars — 95% confidence interval.

results of the chiasma analysis in our studies in F_1 diploid hybrids and those of Albini and Jones, it should be noted that they coincide, although the experiments were performed on different plant material: we used *A. cepa* as a female parent and *A. fistulosum* as a pollinator but Albini and Jones carried out analysis on F_1 hybrids where the female parent was *A. fistulosum* and the pollinator *A. cepa*. Therefore, the influence of the cytoplasm on the configuration of bivalents can be excluded, at least in the case of these closely related species. In both studies, the chiasma localization in the diploid hybrids is most similar to that of the *A. cepa* parent i.e. predominantly in the interstitial and distal regions. Based on observation of SCs, disturbances of synapsis in the centromeric regions of homeologous bivalents between *A. cepa* and *A. fistulosum* usually occurred and, probably, this constraint, reduces proximal chiasma frequency in F_1 hybrid [6]. Authors suggested that these anomalies may indicate sites of DNA differences where extra blocks of DNA occur in the *A. cepa* genome. A further comparison of whole genome sequencing assembled at chromosome-level of the *A. cepa* and *A. fistulosum* genomes will elucidate the cause of disturbances of synapsis in centromere regions of the homeologous bivalents formed by *A. cepa* and *A. fistulosum* chromosomes that differ in size: in average the size of the *A. cepa* chromosome is 2.05 Gb and the size of the *A. fistulosum* chromosome is 1.45 Gb. However, we observed a complete synapsis via immunolocalization of ZIP1 in F_1 diploid hybrid. The adjustment of axis

 doi:10.20944/preprints202212.0307.v1

lengths during synapsis of the parental chromosomes with different length in interspecific hybrids could take place [53,54].

The *A. cepa* × *A. fistulosum* F_1 triploid hybrid, which have a complete diploid set of *A. fistulosum* chromosomes and eight chromosomes of the female parental species *A. cepa*, are an ideal source for testing our hypothesis of a possible genetic control of the distribution of chiasmata. In the F_1 triploid hybrid, bivalents were formed by the *A. fistulosum* homologous chromosomes that have no differences in the length and homology of sequences. Although a significant shift in the localization of chiasmata to the distal and interstitial regions was found (Table 1, Figure 3). Probably, genetic control over chiasma distribution could promote distal and interstitial chiasmata in the F_1 triploid hybrid at the expense of proximally localized chiasmata. Comparative analysis of *mlh1* and *mus81* transcripts in *A. cepa* and *A. fistulosum* showed a high interspecific identity for both transcripts: 99.8% for *mlh1* and 94.2% for *mus81*. A non-synonymous substitution of even one nucleotide will change the amino acid sequence of the protein and, consequently, the function of the gene as recessive or dominant. Thus, genetic control as one of the factors affecting the localization of crossovers can be considered. With Tyramide-FISH mapping we have shown that *mlh1* gene is located on the long arm of chromosome 2 of *A. cepa* [55]. Alien monosomic aditional lines (AMALs) that possess a single chromosome of *A. cepa* within complete diploid set of *A. fistulosum* were developed by Shigyo *et al*. [56,57]. Based on our result, we expect that in alien monosomic addition line with chromosome 2 of *A. cepa* the number of proximal chiasmata will be significantly decreased.

These intriguing results on chiasma localization performed on unique plant materials have triggered a further study of proteins involved in recombination. We analyzed the distribution of the proteins ASY1 and ZYP1 during prophase I of meiosis in *A. cepa*, *A. fistulosum* and their triploid F_1 hybrids. We revealed the peculiarities of loading and unloading of these proteins in Allium. Firstly, ZYP1 is loaded on the meiotic chromosome axes only at the pairing regions similar to Arabidopsis, maize, wheat, barley and rice [24,58–62]. In contrast, in rye, ZYP1 is loaded on unpaired chromosome axes [63,64]. Secondly, ASY1 is unloaded from regions of complete chromosome pairing similar to maize, wheat and rice. In Arabidopsis, barley and rye ASY1 is present at the sites of complete chromosome pairing and a "sandwich" of ASY1 and ZYP1 is formed in pachytene. Thus, the behavior ASY1 and ZYP1 in Allium is most similar to that of maize, wheat and rice.

We did not find the differences in the assembly and disassembly of ASY1 and ZYP1 between *A. cepa* and *A. fistulosum* while the difference between parental species and their hybrids was observed. In diploid F_1 hybrids at pachytene the chromosome pairing delay marked by ASY1 was occurred. These results agree with data obtained by Albini and Jones [6] who observed only 80-90% of the synapsed chromosome at late pachytene in F_1 hybrid between *A. cepa* × *A. fistulosum*. Also homeologous chromosomes in F_1 hybrid quite often failed to synapse with each other or homeologous synapsis was restricted to one bivalent arm [6].

In this study, we visualized two classes of COs on the pachytenes of *A. cepa* and *A. fistulosum* and their diploid and triploid hybrids. It has been previously showed, that MLH1 identified late recombination nodules (LNs) at pachytene that can be recognized as chiasmata in diakinesis [34,35]. According to data in this study and previous research [6], *A. cepa* and *A. fistulosum* have approximately 19 and 15 chiasmata per cell, respectively. Thus, we expected about 19 and 15 MLH1 sites per cell in pachytene. However, we detected fewer signals per cell than expected: *A. cepa* had 6.0 MLH1 signals per cell, while *A. fistulosum* had 2.3 signals per cell. These results can be explained by the high degree of condensation of Allium chromosomes. *A. cepa* has 16.4 Gb of DNA per eight chromosomes. If we assume that each chromosome contains the same amount of DNA, then there are 2.05 Gb DNA per chromosome. It has previously been shown in wheat that approximately 48 MLH1 sites are visualized on 21 bivalents, which is close to the expected number [34]. Wheat has 17 Gb of DNA per 21 chromosomes i.e. 0.8 Gb of DNA per chromosome. Thus,

 doi:10.20944/preprints202212.0307.v1

the reason of a low number of MLH1 detected signals could be the antibody accessibility problem due to a high chromatin condensation of onion pachytene chromosomes.

It has previously been shown that class I and class II of CO pathways are intimately associated in meiosis [32,43]. In Arabidopsis and wheat, the ratio of class I and class II remains constant (85%:15%), despite large disparities in chromosome number and genome size [2,43]. Besides, the crossover events in wheat are shifted towards the distal regions of the chromosomes [65], while in Arabidopsis the crossover events take place along the entire length of the chromosomes [33]. In our study *A. cepa* had 75%:25% ratio of class I marked by MLH1 and class II marked by MUS81, and the crossover events occurred in distal and interstitial regions. *A. fistulosum* with proximal chiasma localization had 25%:75% ratio of class I and class II. An interesting observation, both MLH1 and MUS81 proteins were found in close proximity to each other in *A. fistulosum* and F_1 diploid hybrid at pachytene (Figure 8). Given the limited number of cells available for analysis, more extensive studies are required in the future. We did not find similar works on the localization of meiotic proteins in plants with proximal localization of chiasmata, which makes *A. fistulosum* a unique plant object for further immunocytological analysis.

Expression of *mlh1* and *mus81* showed distinct patterns among parent species (*A. cepa* and *A. fistulosum*), diploid F_1 hybrid and triploid (Figure 9). By-stage patterns of *mus81* and *mlh1* in *A. cepa* and *A. fistulosum* shows significant similarity and clearly distinguish from CN (copy number) patterns in the F_1 diploid hybrid and tripoid. Both *mlh1* and *mus81* in *A. cepa* shows higher CN than *A. fistulosum* in all analyzed stages of meiosis. One explanation could be that *A. fistulosum* and *A. cepa* differ in genome size, *A. cepa* (1C = 16.4 Gb, [49]) having 4.8 Gb more DNA and correspondingly larger chromosomes than *A. fistulosum* (1C = 11.6 Gb, [50]). Recombination is initiated by the formation of DNA double-strand breaks (DSBs) [66]. In many eukaryotes, including plants, only a small proportion (~5%) of DSBs are repaired as COs [67]. *mlh1* and *mus81* involved in two main pathways of CO formation, so larger genome leads to presence more DSBs which are needs to be repaired and as a consequences higher levels of expressions are observed. Another explanation could be a copy number variation of the *mus81* and *mlh1* genes in the genomes of *A. cepa* and *A. fistulosum*. King *et al*. [68] suggested that intrachromosomal tandem duplications contributed to the huge nuclear genome of onion. Although, *mlh1* gene was described as single-copy in many species [69] or single locus [55]. There is no information about copy number of *mus81* gene in plant genomes however it has been reported that genes related to DNA metabolism tend to be lost after gene duplication and remain single-copy [70].

In contrast to *A. cepa* and *A. fistulosum*, F_1 diploid hybrid showed different by-stage pattern of differential expression of both *mlh1* and *mus81* genes. While both in *A. cepa* and *A. fistulosum* maximum values of CN presented in zygotene, in the F_1 diploid hybrid maximum reached in pachytene (Figure 9). This is consisted with a shift in assembly of ASY1 and ZYP1 on chromosomes observed in this work.

Expression pattern of *mlh1* in triploid showed significant difference in comparison with F_1 diploid hybrid as well as both parental species *A. cepa* and *A. fistulosum*. Maximum expression observed in leptotene and constantly decreasing in zygotene and pachytene while both in *A. cepa* and *A. fistulosum* maximum CN observed in zygotene (Figure 9). Expression level of *mus81* affects small changes in the course of prophase I of meiosis but still constantly increasing. This could be explained the presence in triploid an additional set of chromosomes from *A. cepa* which are not involved in bivalents formation. So, an additional portion of transcripts are required that all created DSBs will be repaired on these chromosomes. *mlh1* also is involved in DNA repair [71] so in leptotene stage where maximum expression observed it can be involved in reparation of induced DSBs.

In conclusion, we applied an advanced approach that uses a comparative analysis of chiasma distribution in PMCs, immunolocalization of MLH1, MUS81, ASY1 and ZYP1 on meiotic chromosomes, and *mlh1*/*mus81* gene expression profiling in different stages of meiosis in *A. fistulosum*, *A. cepa* and diploid (2n = *2x* = 8C+8F) and triploid (2n = *3x* =

 doi:10.20944/preprints202212.0307.v1

16F+8C) F_1 hybrids *A. cepa* × *A. fistulosum*. For the first time, the analysis of the frequency and localization of chiasmata in the *A. fistulosum* homologous bivalents in the presence of a complete haploid set of the *A. cepa* chromosomes were performed. We demonstrate a significant shift in the COs localization to the distal and interstitial region in F_1 triploid hybrid. This observation points to a possible genetic control of COs distribution. Analysis of assembly and disassembly SC in *A. fistulosum* and *A. cepa* showed that ASY1 is unloaded from regions of complete chromosome pairing similar to maize, wheat and rice, ZYP1 is loaded on the meiotic chromosome axes only at the pairing regions similar to Arabidopsis, maize, wheat, barley and rice. In diploid F_1 hybrids at pachytene the chromosome pairing delay marked by ASY1 was revealed. Immunolocalization of MLH1 and MUS81, and *mlh1/mus81* gene expression profiling in different stages of meiosis showed a spatiotemporal asymmetry among *A. cepa*, *A. fistulosum* and their diploid and triploid F_1 hybrids. The phenomenon of non-random distribution of chiasmata is determined by many factors, including chromatin organization, epigenetic modification, segment specificity, length of chromosome and genetic regulation.

4. Materials and Methods

4.1. Plant Materials

Perennial plants of *A. fistulosum* (2n = *2x* = 16), variety Ruskiy Zimniy grow on the experimental field of the Center for Molecular Biotechnology RSAU-MTAA. Bulbs of *A. cepa* (2n = *2x* = 16), variety Chalcedon were planted in the field. F_1 hybrids between *A. cepa* and *A. fistulosum* were obtained by manual emasculation of anthers in unopened buds. Pollen from *A. fistulosum* plants were collected in Petri dishes and stored at +4 °C until the pistil stigma ripened for pollination in emasculated buds of *A. cepa*. Pollination of each flower was carried out for 2 days by reapplying pollen on the stigma of the pistil with a brush. F_1 diploid hybrid *A. cepa* × *A. fistulosum* (2n = *2x* = 8F+8C) and F_1 triploid hybrid *A. cepa* × *A. fistulosum* (2n = *3x* = 16F+8C) were used in this study.

4.2. Genomic in situ hybridization (GISH)

Mitotic chromosomes of F_1 hybrids were prepared from young root meristems using the squash method according to Kudryavtseva *et al*. [72]. *In situ* hybridization, immunological detection, and counterstaining procedures were the same as previously described by Khrustaleva and Kik [73]. The hybridization mixture contained: 50% (v/v) formamide, 10% (w/v) dextran sulfate, 2×SSC, 0.25% (w/v) sodium dodecyl sulfate (SDS), 50 ng/μL of labeled probe (DIG)-11-dUTP and 1500 ng/μL of blocking DNA. In the hybridization mixture, we used a ratio of 1:30 of probe and block DNA, and washes at 78% stringency were applied. In F_1 *A. cepa* × *A. fistulosum* (2n = *2x* = 8F+8C) the *A. fistulosum* genomic DNA was used as a probe and the *A. cepa* genomic DNA was used as a block. In F_1 *A. cepa* × *A. fistulosum* (2n = *3x* = 16F+8C) the *A. cepa* genomic DNA was used as a probe and the *A. fistulosum* genomic DNA was used as a block. In both cases the labeled (DIG)-11-dUTP probe DNA was detected with anti-Dig-FITC raised in sheep (Roche diagnostics GmbH, Mannheim, Germany) and amplified with anti-sheep-FITC raised in rabbit (Vector Laboratories, California, USA).

GISH preparations were visualized using a Zeiss AxioImager M2 microscope (http://www.zeiss.com, accessed on 15 November 2021) and black-white sensitive digital Hamamatsu camera C13440-20CU (http://www.hamamatsu.com accessed on 15 November 2021). The final optimization of images was performed using Adobe Photoshop (Adobe Inc., San Jose, CA, USA). Karyotype analysis and identification of individual chromosomes with fluorescent signals by DRAWID program [74] were performed according to bulb onion nomenclature [75] and previously published karyotypes of closely related Allium species [76].

 doi:10.20944/preprints202212.0307.v1

4.3. Analysis of the chiasma distribution in PMCs

Fresh unfixed anthers containing pollen mother cells (PMCs) at metaphase I were tapped out in a drop of 1% acetocarmine on a glass slide, gently mixed, and then heated for 1 min at 60 °C on a heating table. The cells were spread by tapping on the coverslip and gently squashed. Slides were examined under a Zeiss Axiolab 5 microscope (http://www.zeiss.com, accessed on 28 August 2021) using phase-contrast microscopy. The selected images were captured using a digital Axiocam 208 color camera (http://www.zeiss.com, accessed on 28 August 2021). Image processing was performed by Zen 2.6 lite (blue edition) an image analysis software. Bivalent arms were arbitrarily divided into three regions of equal length (proximal, interstitial, distal) and the chiasmata were assigned to these regions by eye in case of undoubted position or the position were measured by DRAWID program [74]. Only non-overlapping bivalents were used for measurements of positions of chiasmata.

Statistical analysis of chiasmatas' location types' distribution was performed applying correspondence analysis using FactorMinerR package v2.5 [77]. Plot was visualized using ggplot2 v3.4.0 package [78]. All steps of analysis and visualization were performed using R v4.2.1 [79].

4.4. Immunochemical analysis

4.4.1. Searching for target proteins (MLH1, MUS81, ZYP1 and CENH3) sequences for antibody production

For the antibody production we performed searching for the sequences of ZYP1 protein (component of central axis of SC), MLH1 and MUS81 which are the key enzymes in plant recombination. Reference transcriptomes of *A. cepa* and *A. fistulosu*m from GenBank (Transcriptome Shotgun Assembly) were used for the acquisition of protein sequences. Sequences of these proteins from other species in order to use as reference were identified based on literature data: ZYP1 (*Zea mays*, GenBank: ADM47598.1, [60]), MLH1 (*Solanum lycopersicum*, GenBank: EF071927.1, [35]), MUS81 (*Arabidopsis thaliana*, GenBank: AB177892.1, [80]). tBLASTn was used for identification transcript sequences of the corresponding proteins in Transcriptome Shotgun Assembly database (identity >50%, query cover >70%). The longest ORF (Open Reading Frame) was translated into aminoacid sequence. The following steps including identification of peptide sequence for antibody production and antibody synthesis were performed by outsource company PrimerBioMed (https://primebiomed.ru/). For CENH3 the previously described peptide was used for antibody synthesis [81].

4.4.2. Preparation of meiotic chromosome for immunostaining

We developed an original method of meiotic chromosome preparation. Anthers at the desired stage of meiosis were fixed by Clark's fixative (ethanol:acetic acid, 3:1, v/v) for the 1 hour. The fixed anthers were washed in the tap water for 30 min and then in citrate buffer (10 mM sodium citrate, 10 mM citric acid) pH 4.8 for 10 min. 5-8 anthers were transferred to 1.5 mL tubes with 50 μL of 0.6% enzyme mixture (1:1:1) pectolyase Y-23 (Kikkoman, Tokyo, Japan), Cellulase Onozuka R-10 (Yakult Co. Ltd., Tokyo, Japan), and Cytohelicase (Sigma-Aldrich Co. LLC, St. Louis, MO 63103 USA) for 120 min at 37 °C. After 120 min the enzyme mixture was removed from the tubes using Pasteur Pipettes. Anthers were gently transformed into a fine cell suspension in the tube using a dissecting needle. The 100 μL of 60% acetic acid was added to the cell suspension. The tube with cell suspension was then heated for 5 min at 50 °C. The 60 μL of ethanol/acetic acid fixative at a ratio of 3:1 were added. A total of 10 μL of cell suspension was dropped onto a slide and by the time the surface became granule-like (10–15 s), 30 μL of ethanol/acetic acid fixative at a ratio of 3:1 was added. Then the slides with cells were immediately dried with an airflow. The same day the slides were used for immunochemical analysis. Some slides were kept in the fridge -70 °C.

 doi:10.20944/preprints202212.0307.v1

4.4.3. Sequential immunostaining with antibodies to ASY1 and ZYP1, MLH1 and MUS81 and CENH3

Slides were incubated with blocking buffer (5% BSA in 1×PBS, 0.1 Tween-20, 1 mM EDTA pH = 8.0) for 2 hours at room temperature. Then slides were incubated with anti-ASY1 (raised in rabbit) and ZYP1 (raised in rat) or anti-MLH1 (raised in mouse) and anti-MUS81 (raised in guinea pig) diluted 5:100 in the same blocking buffer for 24 hours at 4 °C. Slides were washed 4 × 30 min in 1× PBS, 0.1% Tween-20, 1 mM EDTA pH = 8 at room temperature. Slides were incubated with blocking buffer for the 2 hours at room temperature. The secondary antibodies anti-Rabbit Alexa Fluor 555 (raised in Goat) (Abcam plc, Cambridge, CB2 0AX, UK) and anti-Rat Alexa Fluor 488 (raised in Goat) (Abcam plc, Cambridge, CB2 0AX, UK) or anti-Mouse Alexa Fluor 555 (raised in Goat) (Abcam plc, Cambridge, CB2 0AX, UK) and anti-Guinea pig Alexa Fluor 488 (raised in Goat) (Abcam plc, Cambridge, CB2 0AX, UK) diluted 1:100 in blocking buffer were added. After 1 hours of incubation at 37 °C slides were washed 4 × 30 min in 1× PBS, 0.1% Tween-20, 1 mM EDTA pH = 8 at room temperature and mounted in Vectashield antifade medium (Vector Laboratories) with 2 μg/mL DAPI. For sequential immunostaining with antibodies to CENH3 the coverslips were carefully removed by washing for 4 × 30 min in 4× PBS with 0.1% Tween-20, 1 mM EDTA pH = 8 at room temperature. Slides were then washed for 10 minutes in 1× PBS, 0.1% Tween-20, 1 mM EDTA pH = 8 and were incubated with blocking buffer for 2 hours at room temperature. Primary antibodies to CENH3 (raised in goat) were diluted 10:100 in the blocking buffer. Detection with secondary antibodies anti-Goat Alexa Fluor 555 (raised in Donkey) (Abcam plc, Cambridge, CB2 0AX, UK) was performed as described above for MLH1 and MUS81. The microscopy and measuring were performed as described above (see GISH).

4.4.4. MLH1 and MUS81 signals registration and statistical analysis

Among the obtained immunostaining images, pachytenes with at least 2-3 non-overlapping chromosomes were selected. Previously, it was shown that MLH1 and MUS81 are localized on chromosome axes [35,82]. Therefore, only signals localized on the bivalent axes i.e. at the location of the synaptonemal complex (SC) were taken into account. Signals on overlapping chromosomes, as well as signals located on the borders of chromosomes, were considered as background.

Statistical data processing was performed with Student's t-test. Tests are two-sided, and a P-value of 0.05 was set to be statistically significant.

4.5. Microscopy and imaging

The slides were examined under a Zeiss AxioImager M2 microscope (http://www.zeiss.com, accessed on 15 November 2021). The selected images were captured using a digital Hamamatsu camera C13440-20CU (http://www.hamamatsu.com accessed on 15 November 2021). Image processing was performed by Zen 2.6 (blue edition) an image analysis software.

4.6. Gene expression profiling in different stages of meiosis

4.6.1. Total RNA isolation

Flower buds of *A. cepa* L., var. "Haltsedon" (2n = *2x* = 16), *A. fistulosum* L., var. "Ruskiy Zimniy" (2n = *2x* = 16), hybrid of *A. cepa* × *A. fistulosum* (2n = *2x* = 8C+8F), triploid (2n = *3x* = 8C+16F) containing anthers on different stages of prophase I of meiosis (leptotene, zygotene, pachytene) were uses for total RNA isolation. Total RNA was isolated using ExtractRNA (Evrogen, Moscow, Russia) reagent (monophasic aqueous solution of phenol and guanidine isothiocyanate) according to the manufacturer's protocol. 100 μg of flower buds were used for RNA isolation. Samples were homogenized using Eppendorf tube pestles. Concentration and purity of RNA samples were assessed using a NanoDrop Implen N60 spectrophotometer (Thermo Fisher Scientific). The integrity of the RNA was determined using electrophoresis in 2% agarose gel (0.5× TBE, 4.5 V/cm).

 doi:10.20944/preprints202212.0307.v1

4.6.2. cDNA synthesis

The first strand of cDNA was synthesized by reverse transcription using the MMLV RT kit (Evrogen, Moscow, Russia) according to the manufacturer's protocol. 330 ng of isolated total RNA was used for reverse transcription using Poly-dT oligos (Evrogen, Moscow, Russia) in order to selectively enrich samples with mRNAs.

4.6.3. Digital droplet PCR (ddPCR)

The QIAcuity One ddPCR system (Qiagen) was used and all reactions were prepared using QIAcuity Probe PCR Kit (Qiagen). A set of specific primers for *mus81* and *mlh1* genes was designed. Transcripts of the genes were extracted from TSA (Transcriptome Shotgun Assembly) of *A. cepa* and *A. fistulosum* using genomic sequences from *A. cepa* genome assembly [49] based on existing annotation. The primers were designed in order to be able to obtain a PCR product from gene of all origins in hybrids (i.e. without species-specificity) (Table 3). Each reaction (40 μL) contained 4 μL of 4$\times$ Probe PCR MasterMix (Qiagen), 330 ng of cDNA, 0.8 μM of both forward and reverse primers and 2 μL of 20$\times$ Eva488 dye (Lumiprobe RUS Ltd). The cycling conditions were: 95 °C for 2 min, 40$\times$ (95 °C for 15 s, 58 °C for 15 s, 72 °C for 15 s), then 40 °C for 5 min. Number of copies in each probe was calculated using QIAcuity Software Suite 2.0.20.

Table 3. Specific primers for amplification of *mus81* and *mlh1* cDNA using ddPCR.

Gene	GenBank transcripts ID	Primers
mus81	*A. cepa*: GBRQ01006735.1 *A. fistulosum*: GHMM01233510.1	F: ACCATAGCATACGTCCAAAAGT R: TGAACACTGAACTGCTTAAGAAGA
mlh1	*A. cepa*: GBRO01051308.1 *A. fistulosum*: GFAM01047024.1	F: GGGCAGACTAAACTGGGTTT R: TTACAGCATGCATTTTTCTAGCA

Author Contributions: N.K. — investigation, methodology, resources, verification, visualization; A.E. — formal analysis, investigation, writing — original draft; A.P. — investigation; S.S. — investigation; S.O. — investigation; L.K. — conceptualization, data curation, formal analysis, funding acquisition, investigation, methodology, project administration, supervision, writing – original draft. All authors have read and agreed to the published version of the manuscript.

Funding: This research was funded by the Russian Scientific Foundation, grant number 20-46-07005.

Institutional Review Board Statement: Not applicable.

Informed Consent Statement: Not applicable.

Acknowledgments: We thank Professor Glyn Jenkins for the training course on the immunolocalization of meiotic proteins.

Conflicts of Interest: The authors declare no conflict of interest.

Abbreviations

The following abbreviations are used in this manuscript:

CO	CrossOver
DSB	Double-Strand Breaks
PMC	Pollen Mother Cells
GISH	Genomic *in situ* hybridization
CN	Copy Number
SC	Synaptonemal Complex
AMAL	Alien Monosomic Aditional Line
LN	Late recombination Nodules
ORF	Open Reading Frame
HJ	Holliday Junction

 doi:10.20944/preprints202212.0307.v1

References

1. Darlington, C. Meiosis in diploid and tetraploid Primula sinensis. *Journal of genetics* **1931**, *24*, 65–96.
2. Higgins, J.D.; Armstrong, S.J.; Franklin, F.C.H.; Jones, G.H. The Arabidopsis MutS homolog AtMSH4 functions at an early step in recombination: evidence for two classes of recombination in Arabidopsis. *Genes & development* **2004**, *18*, 2557–2570.
3. Lam, I.; Keeney, S. Mechanism and regulation of meiotic recombination initiation. *Cold Spring Harbor perspectives in biology* **2015**, *7*, a016634.
4. Mercier, R.; Mézard, C.; Jenczewski, E.; Macaisne, N.; Grelon, M. The molecular biology of meiosis in plants. *Annual review of plant biology* **2015**, *66*, 297–327.
5. Gray, S.; Cohen, P.E. Control of meiotic crossovers: from double-strand break formation to designation. *Annual review of genetics* **2016**, *50*, 175.
6. Albini, S.; Jones, G. Synaptonemal complex spreading in Allium cepa and Allium fistulosum. III. The F1 hybrid. *Genome* **1990**, *33*, 854–866.
7. Bishop, D.K.; Zickler, D. Early decision: meiotic crossover interference prior to stable strand exchange and synapsis. *Cell* **2004**, *117*, 9–15.
8. Hillers, K.J. Crossover interference. *Current Biology* **2004**, *14*, R1036–R1037.
9. Kleckner, N.; Zickler, D.; Jones, G.H.; Dekker, J.; Padmore, R.; Henle, J.; Hutchinson, J. A mechanical basis for chromosome function. *Proceedings of the National Academy of Sciences* **2004**, *101*, 12592–12597.
10. Muller, H.J. The mechanism of crossing-over. *The American Naturalist* **1916**, *50*, 193–221.
11. Sturtevant, A.H. The behavior of the chromosomes as studied through linkage. *Zeitschrift für induktive Abstammungs-und Vererbungslehre* **1915**, *13*, 234–287.
12. Keeney, S. Mechanism and control of meiotic recombination initiation. *Current topics in developmental biology* **2001**, *52*, 1–53.
13. Moens, P.B.; Kolas, N.K.; Tarsounas, M.; Marcon, E.; Cohen, P.E.; Spyropoulos, B. The time course and chromosomal localization of recombination-related proteins at meiosis in the mouse are compatible with models that can resolve the early DNA-DNA interactions without reciprocal recombination. *Journal of cell science* **2002**, *115*, 1611–1622.
14. Martini, E.; Diaz, R.L.; Hunter, N.; Keeney, S. Crossover homeostasis in yeast meiosis. *Cell* **2006**, *126*, 285–295.
15. Emsweller, S.; Jones, H.; et al. Meiosis in Allium fistulosum, Allium cepa, and their hybrid. *Hilgardia* **1935**, *9*, 275–294.
16. Emsweller, S.; Jones, H.; et al. An interspecific hybrid in Allium. *Hilgardia* **1935**, *9*, 265–273.
17. Armstrong, S.J.; Caryl, A.P.; Jones, G.H.; Franklin, F.C.H. Asy1, a protein required for meiotic chromosome synapsis, localizes to axis-associated chromatin in Arabidopsis and Brassica. *Journal of cell science* **2002**, *115*, 3645–3655.
18. Lambing, C.; Kuo, P.C.; Tock, A.J.; Topp, S.D.; Henderson, I.R. ASY1 acts as a dosage-dependent antagonist of telomere-led recombination and mediates crossover interference in Arabidopsis. *Proceedings of the National Academy of Sciences* **2020**, *117*, 13647–13658.
19. Storlazzi, A.; Xu, L.; Schwacha, A.; Kleckner, N. Synaptonemal complex (SC) component Zip1 plays a role in meiotic recombination independent of SC polymerization along the chromosomes. *Proceedings of the National Academy of Sciences* **1996**, *93*, 9043–9048.
20. Capilla-Pérez, L.; Durand, S.; Hurel, A.; Lian, Q.; Chambon, A.; Taochy, C.; Solier, V.; Grelon, M.; Mercier, R. The synaptonemal complex imposes crossover interference and heterochiasmy in Arabidopsis. *Proceedings of the National Academy of Sciences* **2021**, *118*, e2023613118.
21. France, M.G.; Enderle, J.; Röhrig, S.; Puchta, H.; Franklin, F.C.H.; Higgins, J.D. ZYP1 is required for obligate cross-over formation and cross-over interference in Arabidopsis. *Proceedings of the National Academy of Sciences* **2021**, *118*, e2021671118.
22. Lloyd, A. Crossover patterning in plants. *Plant Reproduction* **2022**, pp. 1–18.
23. Sym, M.; Engebrecht, J.; Roeder, G.S. ZIP1 is a synaptonemal complex protein required for meiotic chromosome synapsis. *Cell* **1993**, *72*, 365–378.
24. Wang, M.; Wang, K.; Tang, D.; Wei, C.; Li, M.; Shen, Y.; Chi, Z.; Gu, M.; Cheng, Z. The central element protein ZEP1 of the synaptonemal complex regulates the number of crossovers during meiosis in rice. *The Plant Cell* **2010**, *22*, 417–430.
25. Zakharyevich, K.; Tang, S.; Ma, Y.; Hunter, N. Delineation of joint molecule resolution pathways in meiosis identifies a crossover-specific resolvase. *Cell* **2012**, *149*, 334–347.
26. De Muyt, A.; Jessop, L.; Kolar, E.; Sourirajan, A.; Chen, J.; Dayani, Y.; Lichten, M. BLM helicase ortholog Sgs1 is a central regulator of meiotic recombination intermediate metabolism. *Molecular cell* **2012**, *46*, 43–53.
27. Ehmsen, K.T.; Heyer, W.D. Biochemistry of meiotic recombination: formation, processing, and resolution of recombination intermediates. In *Recombination and meiosis*; Springer, 2008; pp. 91–164.
28. Lynn, A.; Soucek, R.; Börner, G.V. ZMM proteins during meiosis: crossover artists at work. *Chromosome Research* **2007**, *15*, 591–605.
29. Hollingsworth, N.M.; Brill, S.J. The Mus81 solution to resolution: generating meiotic crossovers without Holliday junctions. *Genes & development* **2004**, *18*, 117–125.
30. Higgins, J.D.; Vignard, J.; Mercier, R.; Pugh, A.G.; Franklin, F.C.H.; Jones, G.H. AtMSH5 partners AtMSH4 in the class I meiotic crossover pathway in Arabidopsis thaliana, but is not required for synapsis. *The Plant Journal* **2008**, *55*, 28–39.
31. Kurzbauer, M.T.; Pradillo, M.; Kerzendorfer, C.; Sims, J.; Ladurner, R.; Oliver, C.; Janisiw, M.P.; Mosiolek, M.; Schweizer, D.; Copenhaver, G.P.; et al. Arabidopsis thaliana FANCD2 promotes meiotic crossover formation. *The Plant Cell* **2018**, *30*, 415–428.

32. Anderson, L.K.; Lohmiller, L.D.; Tang, X.; Hammond, D.B.; Javernick, L.; Shearer, L.; Basu-Roy, S.; Martin, O.C.; Falque, M. Combined fluorescent and electron microscopic imaging unveils the specific properties of two classes of meiotic crossovers. *Proceedings of the National Academy of Sciences* **2014**, *111*, 13415–13420.
33. Chelysheva, L.; Grandont, L.; Vrielynck, N.; Le Guin, S.; Mercier, R.; Grelon, M. An easy protocol for studying chromatin and recombination protein dynamics during Arabidopsisthaliana meiosis: Immunodetection of cohesins, histones and MLH1. *Cytogenetic and genome research* **2010**, *129*, 143–153.
34. Martín, A.C.; Shaw, P.; Phillips, D.; Reader, S.; Moore, G. Licensing MLH1 sites for crossover during meiosis. *Nature communications* **2014**, *5*, 1–5.
35. Lhuissier, F.G.; Offenberg, H.H.; Wittich, P.E.; Vischer, N.O.; Heyting, C. The mismatch repair protein MLH1 marks a subset of strongly interfering crossovers in tomato. *The Plant Cell* **2007**, *19*, 862–876.
36. Li, X.; Zhang, J.; Huang, J.; Xu, J.; Chen, Z.; Copenhaver, G.P.; Wang, Y. Regulation of interference-sensitive crossover distribution ensures crossover assurance in Arabidopsis. *Proceedings of the National Academy of Sciences* **2021**, *118*, e2107543118.
37. Kolas, N.K.; Svetlanov, A.; Lenzi, M.L.; Macaluso, F.P.; Lipkin, S.M.; Liskay, R.M.; Greally, J.; Edelmann, W.; Cohen, P.E. Localization of MMR proteins on meiotic chromosomes in mice indicates distinct functions during prophase I. *The Journal of cell biology* **2005**, *171*, 447–458.
38. Avdievich, E.; Reiss, C.; Scherer, S.J.; Zhang, Y.; Maier, S.M.; Jin, B.; Hou Jr, H.; Rosenwald, A.; Riedmiller, H.; Kucherlapati, R.; et al. Distinct effects of the recurrent Mlh1G67R mutation on MMR functions, cancer, and meiosis. *Proceedings of the National Academy of Sciences* **2008**, *105*, 4247–4252.
39. Holloway, J.K.; Booth, J.; Edelmann, W.; McGowan, C.H.; Cohen, P.E. MUS81 generates a subset of MLH1-MLH3–independent crossovers in mammalian meiosis. *PLoS genetics* **2008**, *4*, e1000186.
40. Heyer, W.D.; Ehmsen, K.T.; Solinger, J.A. Holliday junctions in the eukaryotic nucleus: resolution in sight? *Trends in biochemical sciences* **2003**, *28*, 548–557.
41. Osman, F.; Dixon, J.; Doe, C.L.; Whitby, M.C. Generating crossovers by resolution of nicked Holliday junctions: a role for Mus81-Eme1 in meiosis. *Molecular cell* **2003**, *12*, 761–774.
42. Berchowitz, L.E.; Francis, K.E.; Bey, A.L.; Copenhaver, G.P. The role of AtMUS81 in interference-insensitive crossovers in A. thaliana. *PLoS genetics* **2007**, *3*, e132.
43. Desjardins, S.D.; Ogle, D.E.; Ayoub, M.A.; Heckmann, S.; Henderson, I.R.; Edwards, K.J.; Higgins, J.D. MutS homologue 4 and MutS homologue 5 maintain the obligate crossover in wheat despite stepwise gene loss following polyploidization. *Plant Physiology* **2020**, *183*, 1545–1558.
44. Netzer, D. Greenhouse technique to evaluate pink root disease caused by Pyrenochaeta terrestris. *Euphytica* **1985**, *34*, 385–391.
45. Galván, G.A.; Wietsma, W.; Putrasemedja, S.; Permadi, A.; Kik, C. Screening for resistance to anthracnose (Colletotrichum gloeosporioides Penz.) in Allium cepa and its wild relatives. *Euphytica* **1997**, *95*, 173–178.
46. Tease, C. Cytological detection of crossing-over in BUdR substituted meiotic chromosomes using the fluorescent plus Giemsa technique. *Nature* **1978**, *272*, 823–824.
47. Tease, C.; Jones, G. Analysis of exchanges in differentially stained meiotic chromosomes of Locusta migratoria after BrdU-substitution and FPG staining. *Chromosoma* **1978**, *69*, 163–178.
48. Higgins, J.; Osman, K.; Jones, G.; Franklin, F. Factors underlying restricted crossover localization in barley meiosis. *Annual Review of Genetics* **2014**, *48*, 29–47.
49. Finkers, R.; van Kaauwen, M.; Ament, K.; Burger-Meijer, K.; Egging, R.; Huits, H.; Kodde, L.; Kroon, L.; Shigyo, M.; Sato, S.; et al. Insights from the first genome assembly of Onion (Allium cepa). *G3* **2021**, *11*, jkab243.
50. BARANYI, M.; GREILHUBER, J. Genome size inAllium: in quest of reproducible data. *Annals of Botany* **1999**, *83*, 687–695.
51. Albini, S.; Jones, G. Synaptonemal complex spreading in Allium cepa and A. fistulosum. *Chromosoma* **1987**, *95*, 324–338.
52. Albini, S.; Jones, G. Synaptonemal complex spreading in Allium cepa and Allium fistulosum. II. Pachytene observations: the SC karyotype and the correspondence of late recombination nodules and chiasmata. *Genome* **1988**, *30*, 399–410.
53. Jenkins, G.; Rees, H. Synaptonemal complex formation in a Festuca hybrid. In Proceedings of the Kew chromosome conference II. Alen & Unwin London, 1983, pp. 233–242.
54. Jenkins, G.; White, J. Elimination of synaptonemal complex irregularities in a Lolium hybrid. *Heredity* **1990**, *64*, 45–53.
55. Ermolaev, A.; Kudryavtseva, N.; Pivovarov, A.; Kirov, I.; Karlov, G.; Khrustaleva, L. Integrating Genetic and Chromosome Maps of Allium cepa: From Markers Visualization to Genome Assembly Verification. *International journal of molecular sciences* **2022**, *23*, 10486.
56. Shigyo, M.; Tashiro, Y.; Isshiki, S.; Miyazaki, S. Establishment of a series of alien monosomic addition lines of Japanese bunching onion (Allium fistulosum L.) with extra chromosomes from shallot (A. cepa L. Aggregatum group). *Genes & genetic systems* **1996**, *71*, 363–371.
57. Shigyo, M.; Imamura, K.; Iino, M.; Yamashita, K.i.; Tashiro, Y. Identification of alien chromosomes in a series of Allium fistulosum-A. cepa monosomic addition lines by means of genomic in situ hybridization. *Genes & genetic systems* **1998**, *73*, 311–315.
58. Higgins, J.D.; Sanchez-Moran, E.; Armstrong, S.J.; Jones, G.H.; Franklin, F.C.H. The Arabidopsis synaptonemal complex protein ZYP1 is required for chromosome synapsis and normal fidelity of crossing over. *Genes & development* **2005**, *19*, 2488–2500.
59. Wang, C.J.R.; Carlton, P.M.; Golubovskaya, I.N.; Cande, W.Z. Interlock formation and coiling of meiotic chromosome axes during synapsis. *Genetics* **2009**, *183*, 905–915.

60. Golubovskaya, I.N.; Wang, C.R.; Timofejeva, L.; Cande, W.Z. Maize meiotic mutants with improper or non-homologous synapsis due to problems in pairing or synaptonemal complex formation. *Journal of experimental botany* **2011**, *62*, 1533–1544.
61. Khoo, K.H.; Able, A.J.; Able, J.A. The isolation and characterisation of the wheat molecular ZIPper I homologue, Ta ZYP1. *BMC research notes* **2012**, *5*, 1–13.
62. Phillips, D.; Nibau, C.; Wnetrzak, J.; Jenkins, G. High resolution analysis of meiotic chromosome structure and behaviour in barley (Hordeum vulgare L.). *PloS one* **2012**, *7*, e39539.
63. Mikhailova, E.; Phillips, D.; Sosnikhina, S.; Lovtsyus, A.; Jones, R.; Jenkins, G. Molecular assembly of meiotic proteins Asy1 and Zyp1 and pairing promiscuity in rye (Secale cereale L.) and its synaptic mutant sy10. *Genetics* **2006**, *174*, 1247–1258.
64. Hesse, S.; Zelkowski, M.; Mikhailova, E.I.; Keijzer, C.J.; Houben, A.; Schubert, V. Ultrastructure and dynamics of synaptonemal complex components during meiotic pairing and synapsis of standard (A) and accessory (B) rye chromosomes. *Frontiers in Plant Science* **2019**, *10*, 773.
65. Devos, K.; Dubcovsky, J.; Dvořák, J.; Chinoy, C.; Gale, M. Structural evolution of wheat chromosomes 4A, 5A, and 7B and its impact on recombination. *Theoretical and Applied Genetics* **1995**, *91*, 282–288.
66. Higgins, J.D.; Perry, R.M.; Barakate, A.; Ramsay, L.; Waugh, R.; Halpin, C.; Armstrong, S.J.; Franklin, F.C.H. Spatiotemporal asymmetry of the meiotic program underlies the predominantly distal distribution of meiotic crossovers in barley. *The Plant Cell* **2012**, *24*, 4096–4109.
67. Osman, K.; Higgins, J.D.; Sanchez-Moran, E.; Armstrong, S.J.; Franklin, F.C.H. Pathways to meiotic recombination in Arabidopsis thaliana. *New Phytologist* **2011**, *190*, 523–544.
68. King, J.; Bradeen, J.; Bark, O.; McCallum, J.; Havey, M. A low-density genetic map of onion reveals a role for tandem duplication in the evolution of an extremely large diploid genome. *Theoretical and Applied Genetics* **1998**, *96*, 52–62.
69. Zhang, N.; Zeng, L.; Shan, H.; Ma, H. Highly conserved low-copy nuclear genes as effective markers for phylogenetic analyses in angiosperms. *New Phytologist* **2012**, *195*, 923–937.
70. Blanc, G.; Wolfe, K.H. Functional divergence of duplicated genes formed by polyploidy during Arabidopsis evolution. *The Plant Cell* **2004**, *16*, 1679–1691.
71. Dion, É.; Li, L.; Jean, M.; Belzile, F. An Arabidopsis MLH1 mutant exhibits reproductive defects and reveals a dual role for this gene in mitotic recombination. *The Plant Journal* **2007**, *51*, 431–440.
72. Kudryavtseva, N.; Havey, M.J.; Black, L.; Hanson, P.; Sokolov, P.; Odintsov, S.; Divashuk, M.; Khrustaleva, L. Cytological evaluations of advanced generations of interspecific hybrids between Allium cepa and Allium fistulosum showing resistance to Stemphylium vesicarium. *Genes* **2019**, *10*, 195.
73. Khrustaleva, L.; Kik, C. Cytogenetical studies in the bridge cross Allium cepa×(A. fistulosum× A. roylei). *Theoretical and Applied Genetics* **1998**, *96*, 8–14.
74. Kirov, I.; Khrustaleva, L.; Van Laere, K.; Soloviev, A.; Meeus, S.; Romanov, D.; Fesenko, I. DRAWID: user-friendly java software for chromosome measurements and idiogram drawing. *Comparative cytogenetics* **2017**, *11*, 747.
75. De Vries, J. Onion chromosome nomenclature and homoeology relationships workshop report. *Euphytica* **1990**, *49*, 1–3.
76. De Vries, J.; Jongerius, M. Interstitial C-bands on the chromosomes of Allium-species from the section cepa. In Proceedings of the Allium symposium: EUCARPIA-section vegetables; Proceedings. Institute of Horticultural Research, 1988.
77. Lê, S.; Josse, J.; Husson, F. FactoMineR: an R package for multivariate analysis. *Journal of statistical software* **2008**, *25*, 1–18.
78. Wickham, H. Data analysis. In *ggplot2*; Springer, 2016; pp. 189–201.
79. Team, R.C. R: A language and environment for statistical computing. R Foundation for Statistical Computing, Vienna, Austria. *http://www. R-project. org/* **2013**.
80. Mannuss, A.; Dukowic-Schulze, S.; Suer, S.; Hartung, F.; Pacher, M.; Puchta, H. RAD5A, RECQ4A, and MUS81 have specific functions in homologous recombination and define different pathways of DNA repair in Arabidopsis thaliana. *The Plant Cell* **2010**, *22*, 3318–3330.
81. Nagaki, K.; Yamamoto, M.; Yamaji, N.; Mukai, Y.; Murata, M. Chromosome dynamics visualized with an anti-centromeric histone H3 antibody in Allium. *PLoS One* **2012**, *7*, e51315.
82. Higgins, J.D.; Buckling, E.F.; Franklin, F.C.H.; Jones, G.H. Expression and functional analysis of AtMUS81 in Arabidopsis meiosis reveals a role in the second pathway of crossing-over. *The Plant Journal* **2008**, *54*, 152–162.